HAL open science

Numerical Modeling of a Fluidic Actuator dedicated to Flow Control on an Axial Compressor

Clémence Rannou, Antoine Dazin, Julien Marty, Geoffrey Tanguy, Lionel Castillon, Jérôme Delva

To cite this version:

Clémence Rannou, Antoine Dazin, Julien Marty, Geoffrey Tanguy, Lionel Castillon, et al.. Numerical Modeling of a Fluidic Actuator dedicated to Flow Control on an Axial Compressor. EUCASS-3AF 2022-9ème Conférence Européenne des Sciences Aérospatiales, Jun 2022, Lille, France. hal-03759576

HAL Id: hal-03759576

https://hal.science/hal-03759576v1

Submitted on 24 Aug 2022

HAL is a multi-disciplinary open access archive for the deposit and dissemination of scientific research documents, whether they are published or not. The documents may come from teaching and research institutions in France or abroad, or from public or private research centers.

L'archive ouverte pluridisciplinaire **HAL**, est destinée au dépôt et à la diffusion de documents scientifiques de niveau recherche, publiés ou non, émanant des établissements d'enseignement et de recherche français ou étrangers, des laboratoires publics ou privés.

Numerical Modeling of a Fluidic Actuator dedicated to Flow Control on an Axial Compressor

RANNOU Clémence⋆ and
DAZIN Antoine†, MARTY Julien ⋆, TANGUY Geoffrey†, CASTILLON Lionel⋆, DELVA Jérôme †
⋆*DAAA, ONERA, Université Paris Saclay F-92190 Meudon - France*
clemence.rannou@onera.fr · antoine.dazin@ensam.eu · julien.marty@onera.fr · geoffrey.tanguy@onera.fr · lionel.castillon@onera.fr · jerome.delva@onera.fr
† Univ. Lille, CNRS, ONERA, Arts et Metiers Institute of Technology,
Centrale Lille Institut, UMR 9014-LMFL,
Laboratoire de Mécanique des Fluides de Lille - Kampé de Fériet, F59000, Lille, France

Abstract

The operating range of axial compressors can be limited by unstable flow phenomena such as rotating stall. To improve the so-called surge margin, recent studies demonstrated the benefit of active control by air injection. The frame of this paper is the control system of the single stage compressor CME2, located at the Lille Laboratory of Fluid Mechanics. The goal is to optimally capture the behavior of internal flows within the control device consisting in an isolated fluidic actuator on a flat plate. A numerical methodology is presented taking account computational domain, mesh, numerical methods, and turbulence modeling.

Nomenclature

CAD	Computer Aided Design
δ	Boundary layer thickness (mm)
LE	Leading Edge
Ps	Static Pressure (Pa)
Pt	Total Pressure (Pa)
Q_{inj}	Mass Flow (kg/s)
$RANS$	Reynolds-Averaged Navier-Stokes
SMI	Stall Margin Improvement
Tt	Total Temperature (K)
$URANS$	Unsteady Reynolds-Averaged Navier-Stokes
U_∞	Inlet velocity (m/s)
V	Mean velocity (m/s)
x, y, z	Cartesian coordinates (mm)

1. Introduction

Nowadays flow control is a key technology to improve aerodynamic performance and to achieve the constraints which are imposed to aeronautical engine manufacturers in terms of CO_2 and pollutant emissions. According to Air Transport Action Group (ATAG), a net-zero carbon emissions is the main goal to achieve, pledged by 2050.[1] Increasing the efficiency of axial compressors is undoubtedly always a considerable challenge due to performance limitations related to instabilities such as rotating stall and surge. Rotating stall is developing at the clearance region between the blades and the casing, and arise from the interaction of the tip leakage flow with the main flow. Therefore, control systems acting on the flow near the casing offer an efficient solution to increase the stall safety margin, and thus the compressor operating zone by means of passive devices (modification of the geometry without energy inputs) or active devices (need of an external energy source).

Recent studies have shown that active control by injection of air,upstream of the leading edge of the rotor tip makes it possible to delay the onset of stall. Indeed, active control offers a more efficient solution unlike passive control, which requires complex geometry, is expensive to manufacture and does not accommodate engine cycling and wear

issues. According to the work of Li et al.,[9] the main geometric parameters for fluidic actuator having an influence on the injection performance gain is the axial position: the injection is effective if it occurs close to the leading edge, with better results at +/- 10% of the chord. Moreover, the work of Suder, Hathaway et al.[16] explored the influence of the type of injection, the total quantity of air per injector and in particular the speed or moment of injection. The main conclusions can be drawn as follow: i) The injection speed plays a key role as if this value increases then the incidence of the flow decreases, and the formation of blockages also decreases, due to the re-energization of the flow, allowing the unloading of the blades of the rotor at the head. It is noticed also that the micro-blowing offers a low SMI (Stall Margin Improvement) gain compared to a macro-blowing, but the energy cost of the latter is not insignificant. ii) The total amount of movement injected depends on the optimization of the speed and the injection rate. Two different amounts of air can generate the same SMI.

However, CFD calculations today deal with the complexity of the flows involved and the control devices making it difficult to predict the controlled flow. Recent numerical studies faced this challenging flow control system nevertheless. As an example, according to the work of Bae,[2] the mechanism of synthetic jets located at the tip gap size have been numerically analyzed and especially the tip leakage vortex has been analyzed for a row of blades. The process deflects the flow, improving mixing, and reducing the influence of the tip leakage vortex and increasing the outlet static pressure. Recently, Geng et al.[6] analyzed via a URANS simulation on an isolated row of a rotor the use of micro-injection of air at the rotor head. The injection is carried out upstream of the leading edge in order to deflect the vortex. This type of injection weakens the clearance swirl and increases the stall margin. Additionally, Marty et al.[11] also analyzed the blowing upstream and downstream of the rotor; Neuhaus and Neise[13] focused on continuous air injection for different configurations, showing the benefits on noise reduction with small injection rates or on performance with larger injection rates. All these systems can effectively reduce the loss area generated by the tip leakage vortex, while taking into account the energy required for their operation and the difficult feasibility of implementing such systems on real compressors. Unfortunately, the numerical studies are still confronted with a lack of precision of the results: the velocity gradients are not correctly represented in the previous works due to the limits of the URANS simulations.

The challenge is therefore to better understand the physical mechanisms involved in the appearance of rotating stall such as clearance size, and their control by blowing to the casing, in order to be able to anticipate and optimize the stall margin. Fluidic actuators consist to modify the main flow by injecting a secondary flow: in the present project, air is injected. The flow interaction results in a modification of the aerodynamic performance. By using such advanced actuators for applications such as axial compressors, it is obviously necessary to validate numerical simulations with an experimental approach. The main goal of the present paper is to develop a numerical methodology able to capture the flow behavior delivered by an injector blowing air in a flat plate configuration. This is in the outlook to pursue calculations on the CME2 axial compressor and to investigate the fluid physics parameters with continuous blowing case (no forcing frequency). This configuration corresponds to an experimental case analysed on the test bench at ONERA Lille, and the actuators tested to those installed on the CME2 bench. The approach consists of several objectives:

- Selection of the geometry of the injector in a flat plate configuration
- Analysis of different types of mesh (structured, unstructured, hybrid)
- Comparison of the numerical results with experimental data, for a jet in a boundary layer

The paper is organised as follows: first, the methodology developed for capturing flow behavior within a CFD analysis is described : presentation of the computational domain and the mesh strategy. Then, a reference case is presented with comparison with experimental data. Finally, the optimal methodology is discussed on the benefit to implement it into a real application such as the CME2.

2. Materials and methods

2.1 CME2 Active control system

The considered test-case is the single stage low speed axial compressor CME2 located at the Lille Fluid Mechanics Laboratory (LMFL). The maximum speed is the nominal one, and the value is 6330 rpm. The numbers of blades of the rotor and the stator are respectively 30 and 40, giving a periodicity of $2\pi/10$. More details are given in Veglio's thesis.[17] The air injection system of the CME2 consists of 40 actuators (Figure 1), grouped in pairs on 20 blocks, evenly distributed around the circumference of the compressor. The blow-off is designed to be as close as possible to the rotor blade tips and thus the injection channel is curved at the outlet. This particular shape generates an air outlet tangential to the wall. The jet is therefore stuck to the surface and remains stuck to the wall of the casing, in particular

thanks to the Coandă effect. The center of the actuators is located 10mm from the leading edge of the rotor. Figure 1 presents the general characteristics of the active control system.

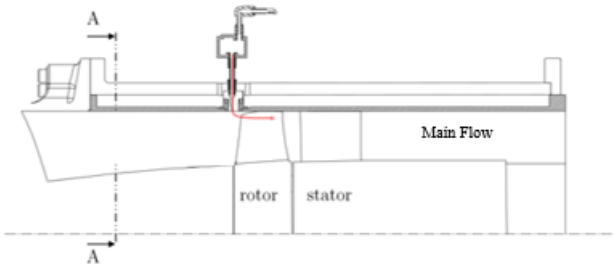

CME2 Injection System	
Number of injectors	40
Axial position	-10 mm
Injection angle (pitch)	0°
Outlet section	5 mm^2

Figure 1: CME2 active control system: longitudinal view (left) and setup characteristics (right)

2.2 ONERA test bench Setup

Onera test bench (30 x 30 cm^2 test cross-section, V_{MAX} = 40 m/s) is dedicated to fluidic actuator characterization, as Figure 2 displays the different parts of the this test bench. The test bench is used as CFD validation for the present project. Indeed, measurements allow to perform calibration of the actuators with test conditions, similar to the CME2 application. It permits also to carry detailed analysis of internal flows with the active flow control. According to the Figure 2 on the right, the characterization of continuous blowing at different massflow rates, from one injector includes two possible experimental planes : longitudinal and transversal velocity fields in order to study the flow behavior experimentally.

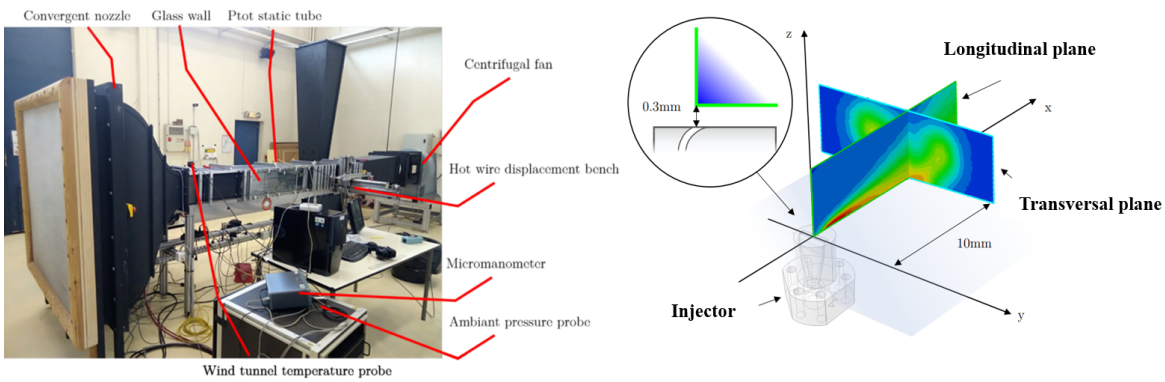

Figure 2: Onera test bench and jet plane characterization of one injector

The following sections present the experimental results of the characterization on the isolated jet at atmospheric pressure, and this will allow a comparison with CFD ones, in order to validate the mesh strategy carried out. It can be noticed also that these preliminary results are closer to the compressor case without obviously strong crossflows linked to the CME2 environment. This will provide in fact a first reference to describe the behavior of the flow in presence of the injector.

2.3 Numerical setup

2.3.1 Presentation of the flat plate geometry

Simulations of a real injector for the control on the CME2 were carried out with different meshing strategies. The objective is to compare the results of the numerical simulation with those of characterization tests of the injector obtained on the ONERA Lille test bench. For the simulations, the injector was meshed from the initial CAD as Figure 3 illustrates. The jet emerges in a flow at a speed according to the case of the study, hence in a jet in a boundary layer, at a fixed speed representative of a case on the CME2 bench (U_∞ = 40 m/s), modeled with a long configuration. Extension was created with Pointwise software in order to relate to a flat plate configuration. A preliminary larger configuration has been designed with the following dimensions: (Lx, Ly, Lz) = (1400, 600, 300) mm for the case with a jet in boundary layer at U_∞ = 40 m/s to correspond with experimental data.

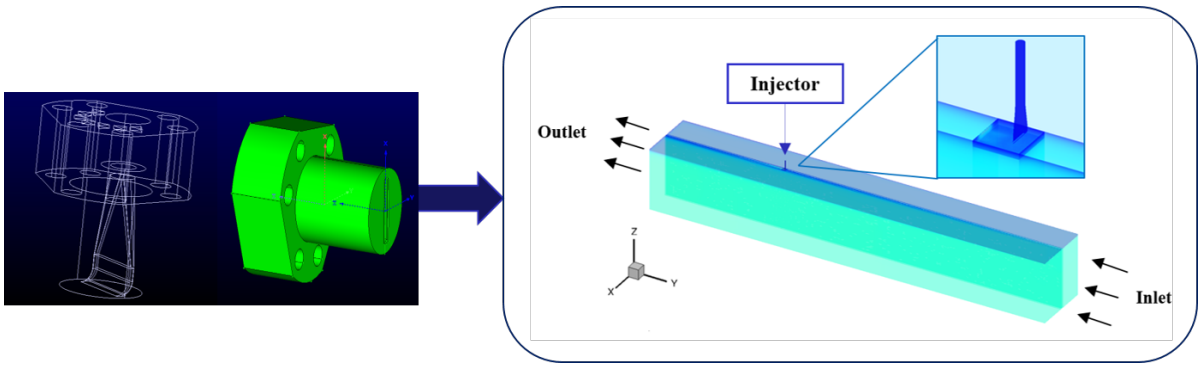

Figure 3: Flat plate configuration with one actuator

2.3.2 Mesh strategy

Different types of mesh have been undertaken in order to identify the best strategy for the CME2 case. The considered three types of mesh, precisely structured, unstructured and hybrid mesh are characterized as follows:

- Structured: The size of the first wall cell is 5 μm, as well as a number of layers for the boundary layer of 15. The mesh is coincident with hexahedra. The number of mesh cells used is 16.0 10^6.

- Hybrid: The mesh was produced with a first wall cell size of 5 μm, and a number of layers in the boundary layer of 15. The mesh is composed of prisms / pyramids / tetrahedra at the interface between the injector and the flat plate. All the injector is meshed with hexahedra and as been processed in unstructured method by the software Pointwise. The rest is composed of hexahedra for the flat plate considered as the structured part. It is composed of 33.29 10^6 mesh cells.

- Unstructured: It results from the hybrid mesh with the structured part which has been processed by converting the elements into unstructured under Pointwise. The injector part and the interface are therefore composed of hexaedra and prisms / pyramids / tetrahedra respectievely. The number of mesh cells used is 33.29 10^6.

For these reference meshes, the magnitude y + is less than 1 near the walls. Following figures present the main specific characteristics between the Hybrid/Unstructured and Structured mesh. It can be noticed the difficult parts to mesh and which required particular attention for meshing, in particular at the level of the circular edge of the injection and at the base of the injection with the particular angled shape. Subsidiary construction lines of Bezier curve types were necessary in order to be able to carry out the mesh under Pointwise.

2.3.3 Presentation of numerical parameters

Calculations are performed with the elsA solver,[3] developed at ONERA and co-owned by ONERA and SAFRAN. This code relies on a cell-centered finite-volume discretization on structured multi block meshes. A convergence study has been conducted in order to study the compromise between computational cost and reliability considering each type of mesh. Reynolds-Averaged Navier-Stokes equations are solved for compressible flows. Ideal gas law characterizes the fluid with the Sutherland's law for the viscosity. The heat fluxes are computed with the Fourier's law and diffusive fluxes are calculated with a classical second-order-centered scheme. Turbulence is modeled with the Spalart-Allmaras mode.[15] The Roe solver is used as second order centered space discretization in order to compute the transport equations of turbulence models. Time integration is solved by a backward Euler scheme. Local time stepping is also applied to enhance the convergence rate in steady flow conditions. The boundary conditions that have been implemented are summarized in Table 1. Figure 6 illustrates the distinct parts of the domain associated to a specific color for each boundary condition. Walls are shown in blue, the outlet of the domain is presented in red, wall with slip conditions are colored in green,the injection inlet is in blue, and in dark green remains the inlet of the domain.

2.3.4 Turbulence modelling

As seen previously, the Spalart-Allmaras (SA) model was chosen because of its robustness. A single transport equation for the turbulent viscosity is sufficient by neglecting the turbulent kinetic energy in the constitutive law. In this section, this choice is justified by comparing different turbulence models, namely the two-equation $k - l$ model of Smith[14]

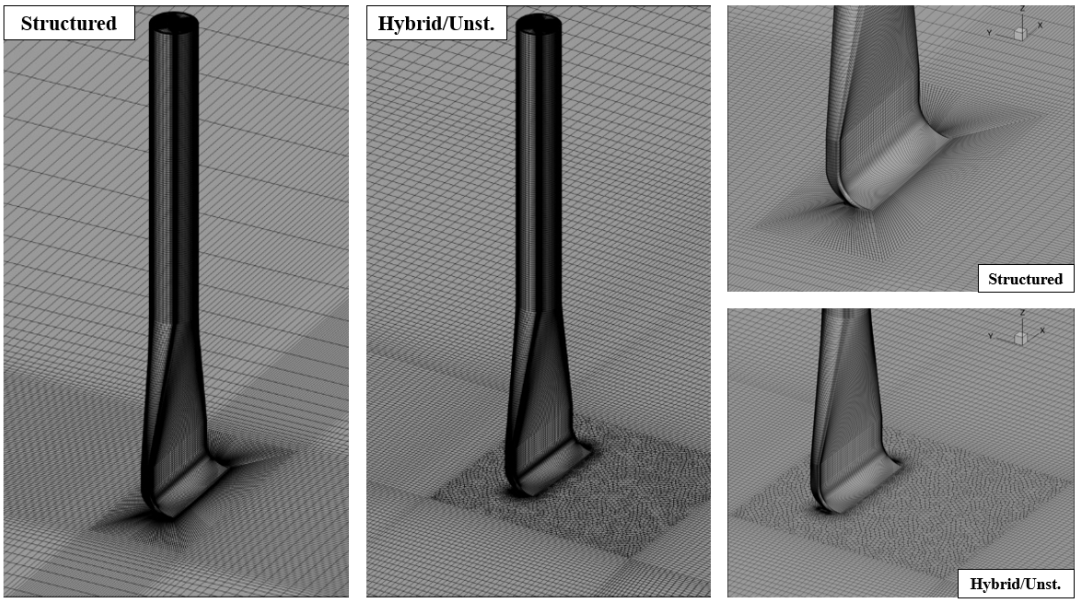

Figure 4: Injector and the interface with the fat plate for Structured and Hybrid/Unstructured mesh

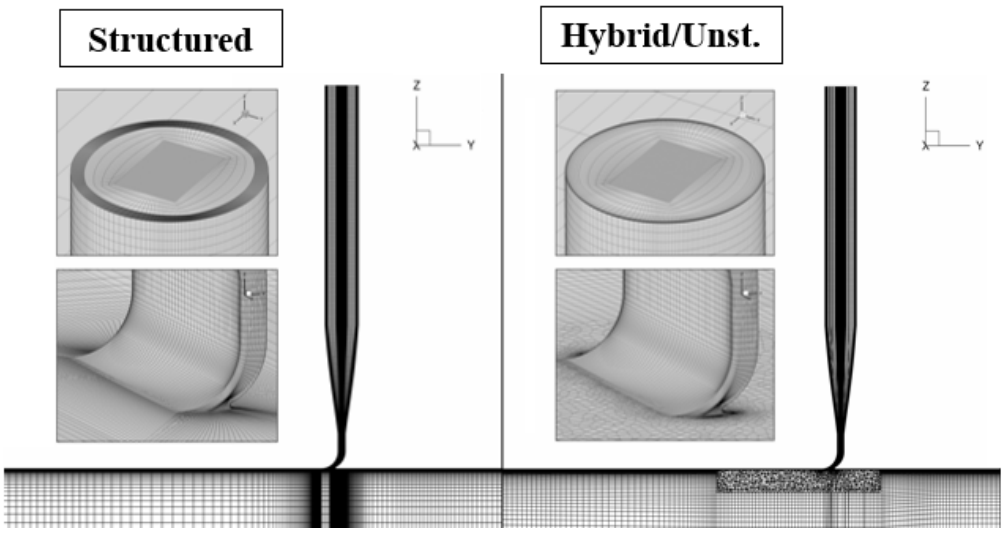

Figure 5: Focus on the Structured and Hybrid/Unstructured mesh of the inlet of the injector and the interface with the flat plate

Table 1: Boundary conditions

Inlet (dark green)	Subsonic inlet condition with prescribed total pressure: - Axial flow direction, - P_t = 101325 Pa, T_t = 288 K
Inlet of the injector (orange)	Subsonic inlet condition with prescribed mass flow rate: - Flow direction normal to boundary: - Q_{inj} = 20, 50, 80 L/min, T_t = 288 K
Flat plate, injectors walls (blue)	Adiabatic wall conditions
Adjacent Wall (green)	Wall-slip conditions on lateral and external frontiers
Outlet (red)	Subsonic inlet condition with prescribed total pressure: - U_∞ = 40 m/s

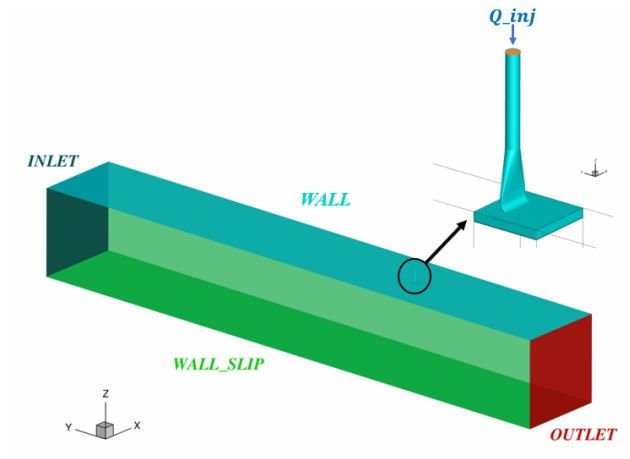

Figure 6: Boundary conditions of the flat plate configuration

based on the work of Rotta in order to calculate in a simplified way the turbulent kinetic energy in the viscous underlayer, the $k-\omega\ SST$ model of Menter[12] with the SST correction to limit turbulent viscosity, and the $k-\epsilon$ model of Launder and Spalding.[8] Only the cases for 20l/min of injection rate are reported in Figure 7 presenting Mach number fields for the different turbulence models and for cases with jet in boundary layer. Optimal results are provided using the Spalart-Allmaras model, $k-l$ model, and $k-\omega\ SST$ model by keeping the jet closer to the wall according to the longitudinal view. Regarding the transverse view, the jet seems further along the wall compared to other models. In addition, residuals have been post-processed for this case with jet in boundary layer. It has been noticed that the Spalart-Allmaras model is the approach that reaches the lower residuals than the rest of the other models. Hence, the Spalart-Allmaras model is always presenting a finer convergence quality and retains a jet more stuck to the wall than the rest of the simulations. By increasing the injection rate, it has been noticed many instabilities, especially at 100 L/min with higher residuals. Future simulations are therefore carried out with this model.

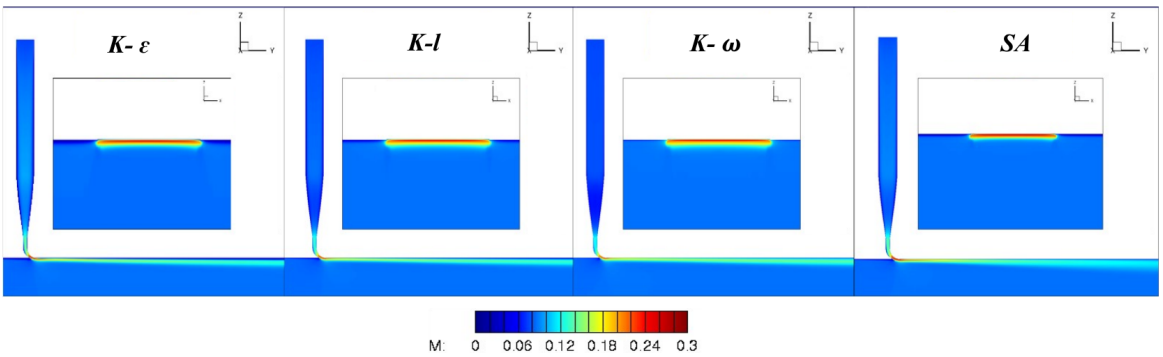

Figure 7: Mach number fields of the turbulence models tested on the flat plate ($k-\epsilon$, $k-l$, $k-\omega\ SST$, SA) in jet in boundary layer

3. Results and discussion : Numerical method evaluation

3.1 Reference case based on structured mesh

The reference case corresponds to the structured mesh configuration as this approach has provided in the past excellent results with elsA code. The simulations investigate a range of mass flow rates for the injector corresponding to the case of the experimental test campaign: Q_{inj} = 20 L/min, 50 L/min, 80 L/min. This refers to a jet in a boundary layer, at a fixed speed representative of a case on the CME2 bench, fixed at U_∞ = 40 m/s. At these conditions, longitudinal and transverse fields were post-processed at these three massflow rates. It has to be noticed that z = 0 mm corresponds

to a position at 0.3 mm from the wall in order to correspond to experimental data. Figure 8 illustrates the specific planes to post-process the numerical calculations. Figure 8 a) and b) present the planes used for the analysis of velocity flow topology, whereas Figure 8 c) represents the slice (y = 280 mm), used for the study of velocity boundary layer to compare with experimental data.

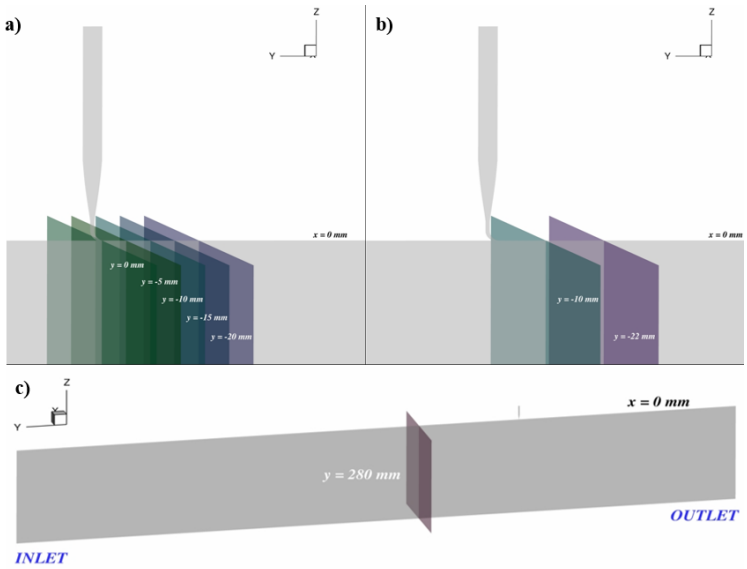

Figure 8: a) and b) Post-processing planes in a longitudinal (slice x = 0 mm) and transversal (slice y = 0, -5, -10, -15, -20 mm) view. c) Post-processing planes in a longitudinal (slice x = 0 mm) and transversal (slice y = 280 mm) view

3.1.1 Analysis of the velocity boundary layer

From the Onera test bench, a flow velocity characterization has been provided at a fixed speed (U_∞ = 40 m/s). Post-processing has been conducted at the same condition than experimental data. Figure 9 compares the experimental results to the numerical ones with structured mesh plotting U/U_∞ as a function of Z/δ. The three cases with injector massflow rates (Q_{inj} = 20 L/min, 50 L/min, 80 L/min) are reported but the injection is not interfering with the results as the post-processing is upstream of the injector. Good agreements are obtained as the numerical boundary layer thickness is nearly reached in a distance of 20 mm, with a same trend than in real conditions. However, it can be noticed a slightly overestimation of the numerical data compared to the experimental ones from U/U_∞ equal from 0.5 to 0.95. Than, numerical data are lower with a discrepancy less than 0.1%. The results obtained for the reference case based on structured mesh demonstrate a reasonably good agreement with the experimental data in terms of boundary layer estimation. Flow topology downstream of the injector is presented in the following section in order to confirm if the jet in boundary layer is correctly captured.

3.1.2 Analysis of the flow topology

To determine the evolution of the flow, two transversal planes (y = -10, -22 mm) have been processed and in addition one in a longitudinal plane at x = 0 mm. Figure 10 presents the velocity fields of transversal planes with experimental data on the left and RANS results on the right, at the same boundary conditions (20 L/min, 50 L/min, 80 L/min). Velocity fields at slice y = -10 mm and -22 mm are well captured by the numerical data with acceptable convergence and massflow rate stabilization. Looking at the experimental data, it can be seen that the injection is not perfectly axial over the entire length of the slot. The presence of lobes is also visible on either side of the position at x = 0 mm, signs that the jet is rolled up on itself. Looking at the RANS results, agreement is reached for the transverse velocity field with numerical fields that present this particular characterization of the jet rolling up into lobes. According to the cases at 50 L/min, the numerical fields cover nearly 4 mm in the center of the slot, as the experimental cases are experiencing also. For the cases at 80 L/min, the jet extents to a little less than 8 mm. Hence, the jet does not occupy the entire injector slot, designed with an oblong section of 10 × 0.5 mm at the outlet. The change of the injection channel can explain also this experimental flow behavior that is not axial, as the inlet of the injector starts with a circular section of 4 mm and ends with the particular oblong section. Figure 11 presents three longitudinal velocity fields at the three distinct massflow rates with experimental results (left) and numerical ones (right). The curved geometry of the injector

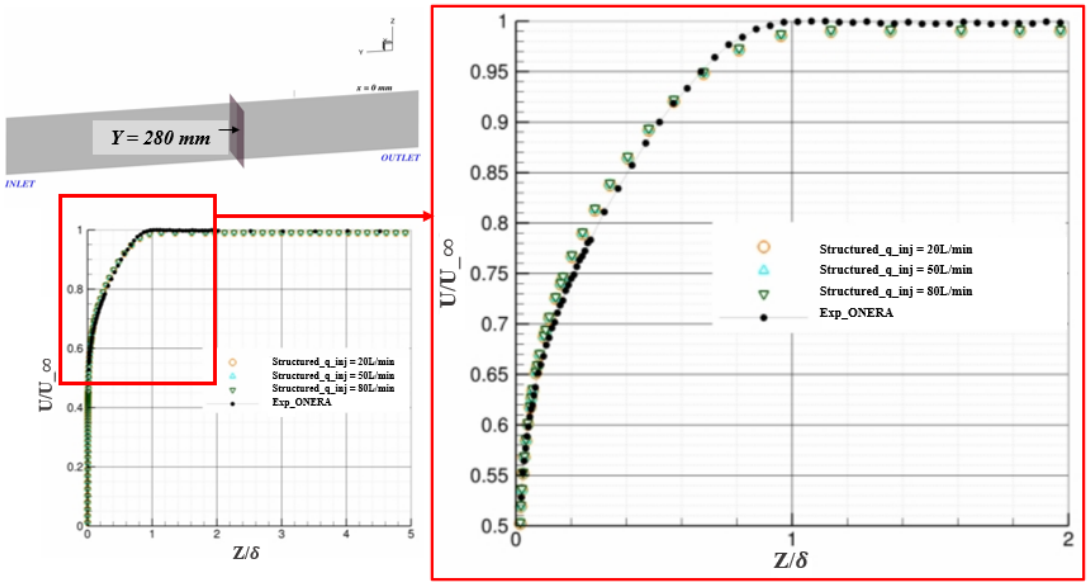

Figure 9: Velocity boundary layer for structured case compared to experimental data

outlet allows the Coandă effect at each massflow rates. Indeed, at the outlet, the jet at high-speed is pressed against the wall, allowing injection at a pitch angle close to zero. Similarly, the numerical jet emerges into the main flow and remains generally close to the wall, being more slightly flared compared to the experimental data. In addition, it seems that at higher massflow rates, the jet velocity is much higher in the numerical results than in the experimental ones. This is particular noticeable at the outlet of the injector especially at 50 L/min and 80 L/min. For this last case, the jet is experiencing a longer distance at velocity higher than 180 m/s (nearly 5 mm) compared to experimental jet (nearly 3 mm). The numerical results seem to therefore slightly overestimate the velocity and respecting the trend of the experimental jet. Therefore, the case with structured mesh provides excellent results compared to experimental data, and captures well the jet flow behavior in a boundary layer.

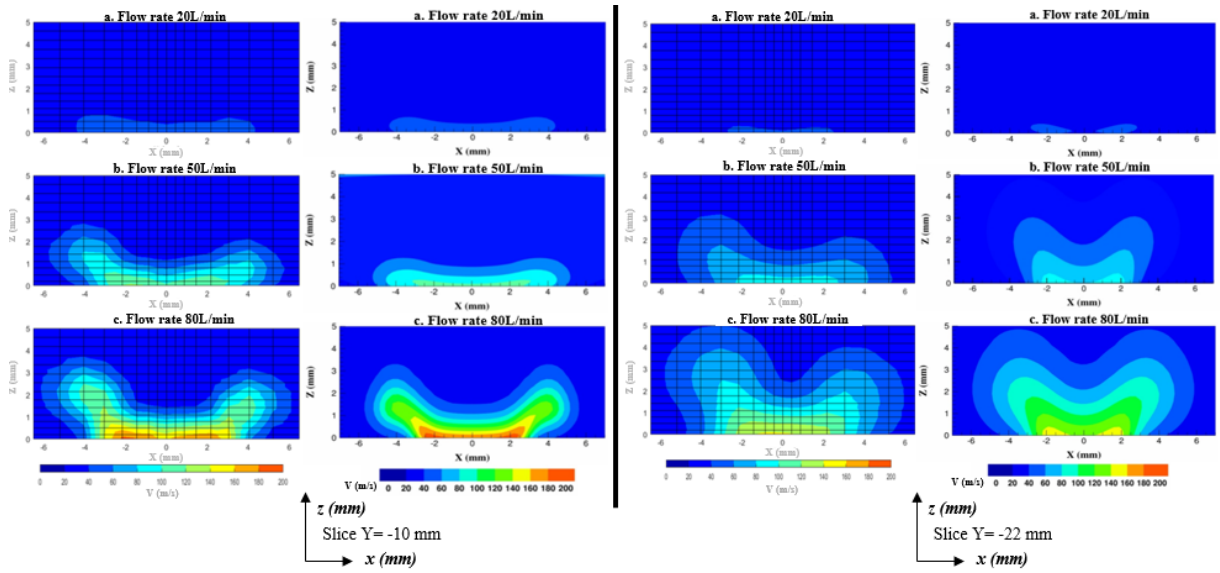

Figure 10: Transversal view at slice y = -10 mm and slice y = -22 mm of the experimental velocity fields (left) compared to numerical one (right)

Further analysis on the flow topology can be conducted : Figure 12 presents numerical transversal velocity fields at 20 L/min and 80 L/min. Streamlines are represented at different y-slices in order to capture the flow behavior near the jet at the outlet of the injector. At 20 L/min, flow recirculation appears from either side of the jet with flow rolling

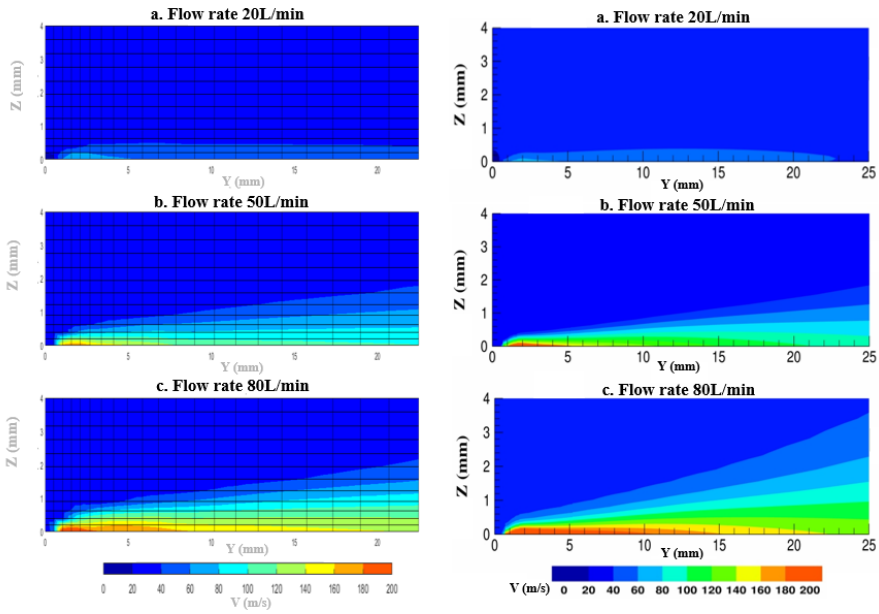

Figure 11: Longitudinal view at slice x = 0 mm of the experimental velocity fields (left) compared to numerical one (right)

up on itself along all the jet. However, regarding at 80 L/min, close to the outlet of the injector, vortex structures are clearly observable at the outermost of the jet when the injection flow is mixing with the main flow. Farther from the jet, few flow recirculation in the x-axis is visible compared to the case of 20L/min, as the jet massflow rate is stronger.

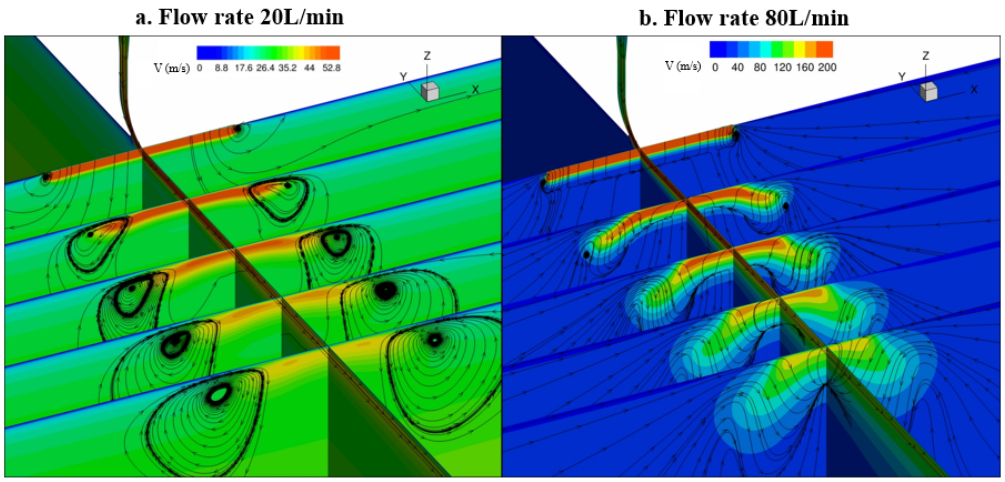

Figure 12: Velocity fields in transversal view with friction lines at massflow rates 20 L/min and 80 L/min

3.2 Application to the CME2 test bench

3.2.1 CME2 geometry complexity and mesh adaptation

When approaching the 360° configuration of the CME2, it is necessary to consider other geometric problems. For instance, the cylindrical configuration of the CME2 and the radius of the rotor have to be respected to perform multi-blocks on CME2 in 360° configuration. This leads to consider specific techniques of meshing in order to respect these conditions. Investigations have been carried out on unstructured and hybrid mesh. The unstructured mesh is simple to perform for this kind of geometry with an interface between the injector and other surface which required particular attention with curves. This can be simply implemented with prisms/pyramids/tetrahedra elements. However, the cost of this strategy might be expensive. The section 3.2.5 will discuss of computational cost compromise of each mesh

technique. Indeed, unstructured approach is more expensive at the iteration and this method takes many more cells than for the structured one. The calculation is hence so much more expensive. Regarding the hybrid, it has the advantage of being able to keep the structured mesh of the vein and to add the injector via an unstructured mesh of it and the zone of intersection with the vein (this zone is very limited in space). The additional cost of the generated calculation should be compensated by the quality of the results, based on the numerical work carried out in the ACONIT project. Indeed, if the number of unstructured cells is relatively lower compared to the one of structured cells, the additional CPU cost linked to the unstructured will undoubtedly be compensated. Another approach can be considered, namely the chimera which is a strategy based on overlapping volumes and interpolations between them. For this case, it requires buffer blocks which leads to a higher number of cells than that of the hybrid mesh and raises the question of the memory allocated to the calculation with elsA code when it deals with 360° configuration : the use of buffer blocks will cost more than for the hybrid method. In addition, the main concern is that the method is not conservative in terms of massflow rate. Therefore, this technique would not be investigated for the CME2 case.

3.2.2 Numerical results with hybrid mesh

Figure 13 compares the experimental results to the numerical ones with plotting U/U_∞ as a function of Z/δ for the hybrid mesh. It can be noticed the RANS results are slightly above the data looking at U/U_∞, from 0.53 to 0.98 with a discrepancy of nearly 0.01%. From nearly Z/δ from 1 to 2, the experimental data are higher compared to the numerical results, with a small difference of 0.01%. In overall, RANS data are corresponding to the experimental data and provide satisfying results. In addition, the hybrid case seems to correspond to the case of structured mesh with a slight overestimation of the velocity ratio from 0.5 to 0.95. Above 0.95, it seems to give better results with less underestimations of the data. Good agreements have thus been provided by the hybrid mesh. Moreover, flow topology can be analysed and be compared to experimental data. Figure 14 illustrates the velocity flow of transversal planes with experimental data on the left and RANS results on the right, at 20 L/min, 50 L/min, 80 L/min. The numerical velocity fields present characteristics very close to the experimental ones whatever the numerical configuration considered. In regard with the case of structured mesh, the velocity fields present the same specific lobes on either side of the position at x = 0 mm. That means the behavior of jet rolling up on itself is well captured. This is observable for both slice y = -10, -22 mm. At 20 L/min, a characteristic low relative velocity region is displayed for each slice as for the experimental data, respecting the length of the jet. Looking at the cases at 50 L/min, the experimental cases cover nearly 4mm in the center of the slot and the RANS results show the same trend. At 80 L/min, the experimental jet length is nearly 8 mm as the one from the numerical results extents also at the same value. Moreover, it is noticeable that the velocity is higher in the numerical data compared to the experimental data, as it has been specified also for the structured mesh. According to the longitudinal velocity fields, presented by Figure 15 for 20 L/min, 60 L/min, 100 L/min, with experimental results (left) and numerical ones (right). As seen for the structured mesh, the Coandă effect at each massflow rates is well captured. The numerical jet is close to the wall especially for the lower massflow rate. For 80L/min, the jet is more diffused compared to the experimental data. Additionally, the RANS simulations slightly overestimate velocity. This trend is also observed for the structured mesh. Indeed, at 80 L/min, the lenght of the jet at a velocity higher than 180 m/s is approximately 5 mm compared to experimental jet with a length of nearly 3mm. Hybrid case seems to much overestimate the velocity data compared to the structured one.

This is confirmed in section 3.2.4, by Figure 3.2.4, illustrating a comparison between the structured and the hybrid case at the configuration at y = -10 mm and y = -22 mm. The data are close to each other at lower massflow rate and especially looking at the curves at y = -10 mm. At higher massflow rates, at y = -22 mm, the discrepancy is nearly 20 m/s at 1 mm, whereas at y = -10 mm, the difference is only 5 m/s. Hence, hybrid mesh provides acceptable results as the structured mesh and can be an interesting solution for the CME2 case.

3.2.3 Numerical results with unstructured mesh

Unstructured case has been also analysed in terms of velocity boundary layer, regarding Figure 16. RANS results are slightly the same than the one from the hybrid case. The values are overestimated compared to experimental data with a discrepancy of nearly 0.01% from U/U_∞ equal from 0.5 to 0.95. Above this limit, the experimental data are a little bit higher than the numerical data. Figure 17 provides the velocity flow of transversal planes with experimental data on the left and RANS results on the right, at the different massflow rates. Unstructured case generates results similar to the experimental ones whatever the numerical configuration considered but the unstructured mesh is providing less quality for the visualization of the results. Similarly, Figure 18 shows the velocity flow of longitudinal planes with experimental data on the left and RANS results on the right, at different massflow rates (20 L/min, 50 L/min, 80 L/min). The results are likely the same than the ones from the hybrid mesh cases, and correspond to the experimental data.

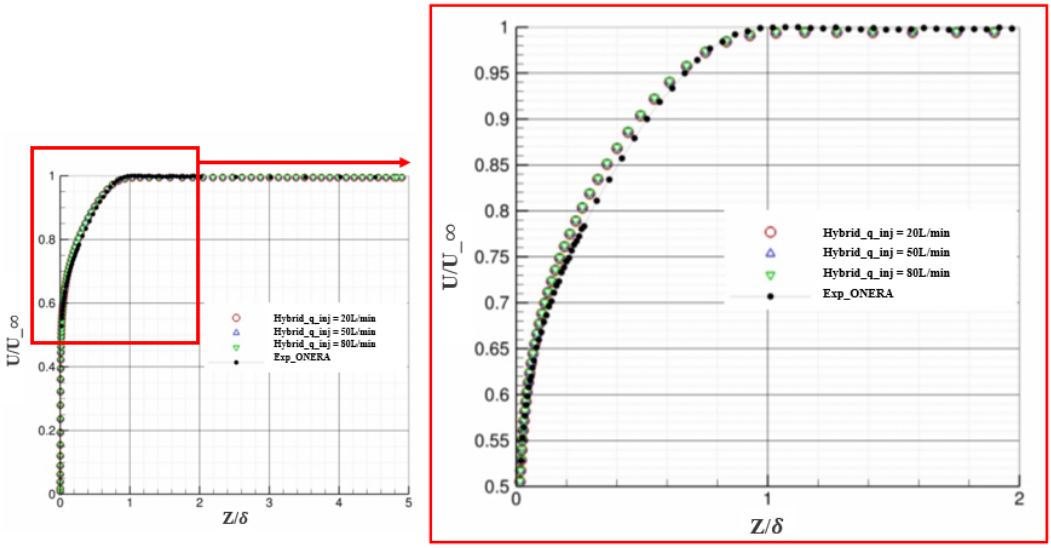

Figure 13: Velocity boundary layer for hybrid case compared to experimental data

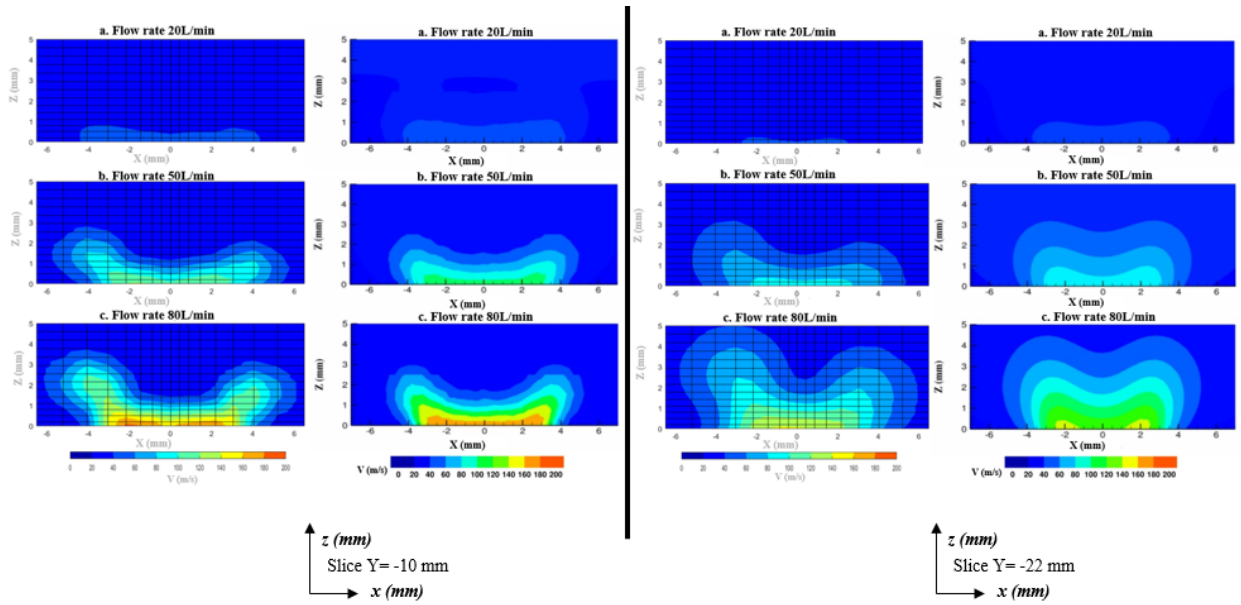

Figure 14: Transversal view at slice y = -10 mm and slice y = -22 mm of the experimental velocity fields (left) compared to numerical one (right)

3.2.4 Comparison of the velocity fields for the different mesh case

In this section, velocity has been analysed for each slice investigated, i.e the transversal slice y = -10 mm, y = - 22 mm at x = 0 mm, and the longitudinal slice X = 0 mm at y = 0 mm, in order to compare values between the specific mesh techniques to the experimental data. Regarding Figure 19, it can be noticed that acceptable agreement is reached for all the cases: at each massflow rate (20, 50, 80 L/min), the curves are following the same trend in respect of the wind tunnel data. The values from hybrid and unstructured are almost the same and are generally above the test data. Moreover, there is a higher discrepancy observable between structured and hybrid/unstructured mesh case. The structured cases are globally provided accurate results with velocity values similar to the experimental data with a slightly difference as these numerical results are still higher. For each mesh approach, the discrepancies with test data are accentuated as the massflow rate is higher, especially looking at the transversal slices in the region of z equal at 0 to 1 mm. For z superior to 1, excellent results are shown with experimental data corresponding to numerical ones in overall.

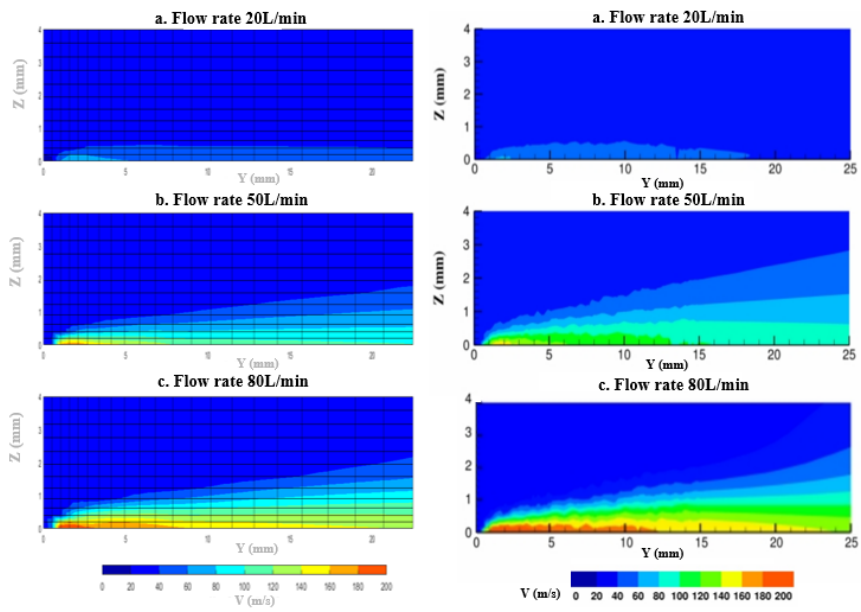

Figure 15: Longitudinal view at slice x = 0 mm of the experimental velocity fields (left) compared to numerical one (right)

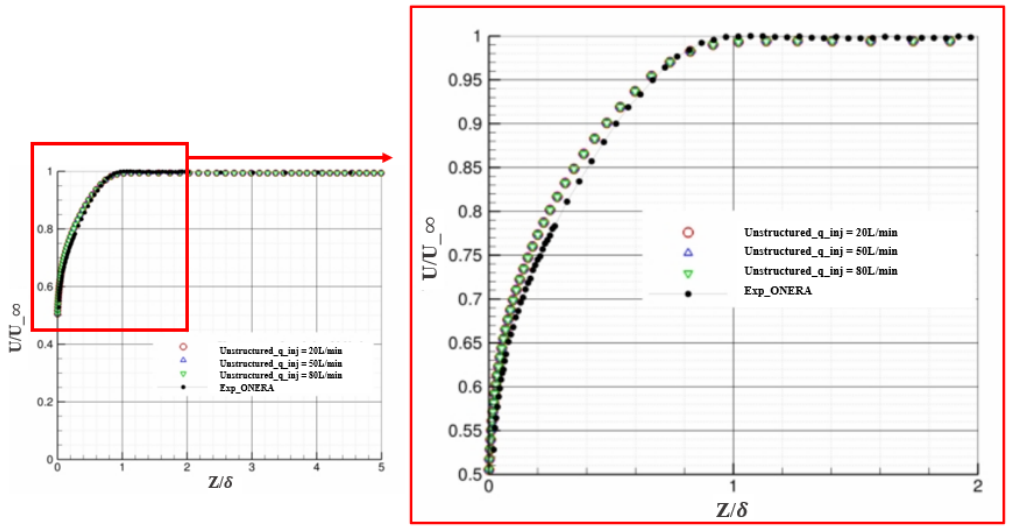

Figure 16: Velocity boundary layer for unstructured mesh compared to experimental data

3.2.5 Comparison of the different mesh computational cost

Relative CPU costs and allocated memory requirements are presented in function of the specified cases of structured, hybrid and unstructured calculations. Indeed, the relative CPU cost is taking into account the number of cells corresponding to each mesh strategy, iterations and cores allocated for the calculations whereas the relative memory cost is only defined by the number of cells. Table 2 summarizes the main characteristics of numerical performance. According to this table, some conclusions can be drawn as follows:

- Unstructured case is the longest and most expensive mesh approach in memory : it represents twice time the cost of structured mesh in terms of computational memory.
- Hybrid and structured meshing methods have the advantage to present a relatively lower CPU cost and are not presented an expensive computational cost.
- Structured mesh presents good results in terms of computation cost with one half than the number of mesh of the hybrid one.

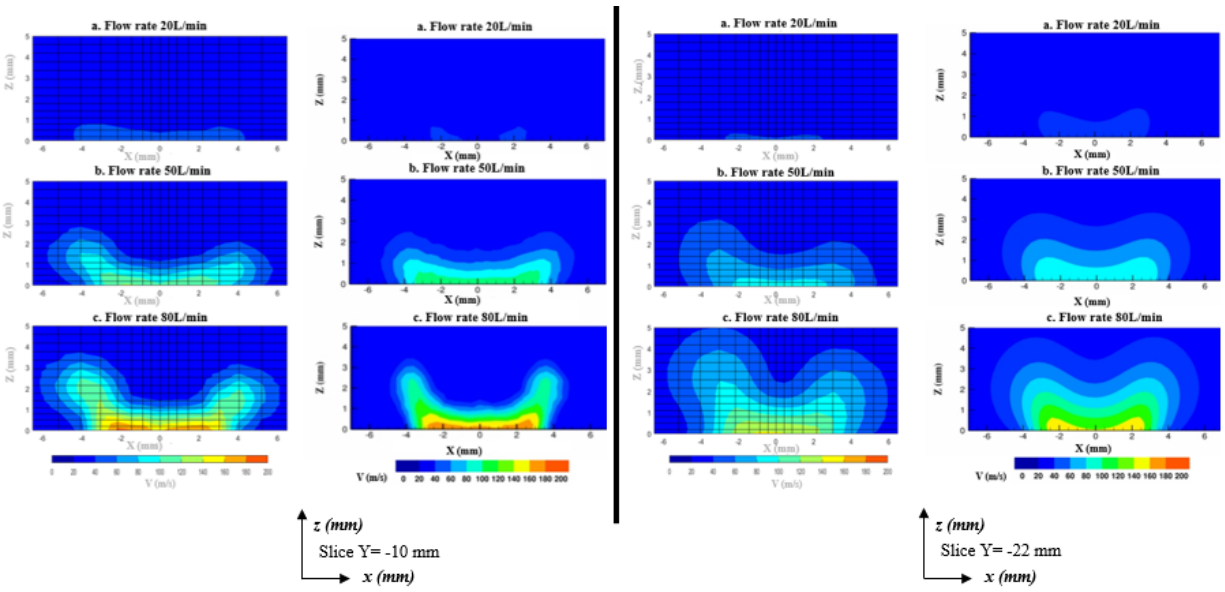

Figure 17: Transversal view at slice y = -10 mm and slice y = -22 mm of the experimental velocity fields (left) compared to numerical one (right)

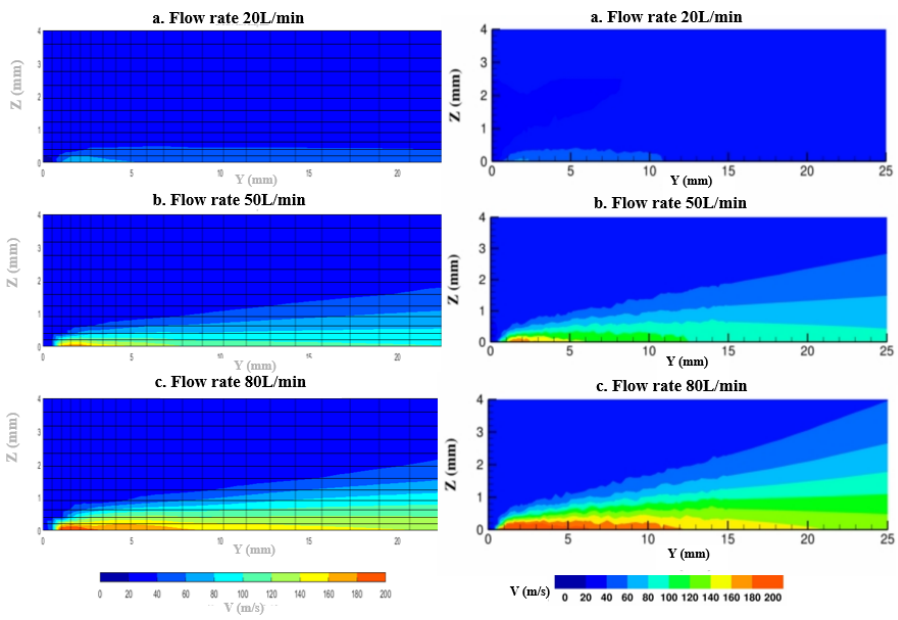

Figure 18: Longitudinal view at slice x = 0 mm of the experimental velocity fields (left) compared to numerical one (right)

Strategically, the reasonable choice is rather towards the structured with the quality of the results and due to the time and cost of calculation memory compared to the other mesh methods. However, due to the complexity of the CME2 geometry, hybrid mesh will be chosen for future calculations as the computational cost is closed to the structured mesh and numerical results are satisfying compared to ones from the test campaign.

4. Conclusion

Preliminary meshes were carried out on a flat plate configuration with an injector which included delicate parts to mesh. Three types of meshes were investigated such as the structured, the hybrid and the unstructured one. Each type of mesh has provided numerical results leading to the following conclusions : Structure mesh is the optimal

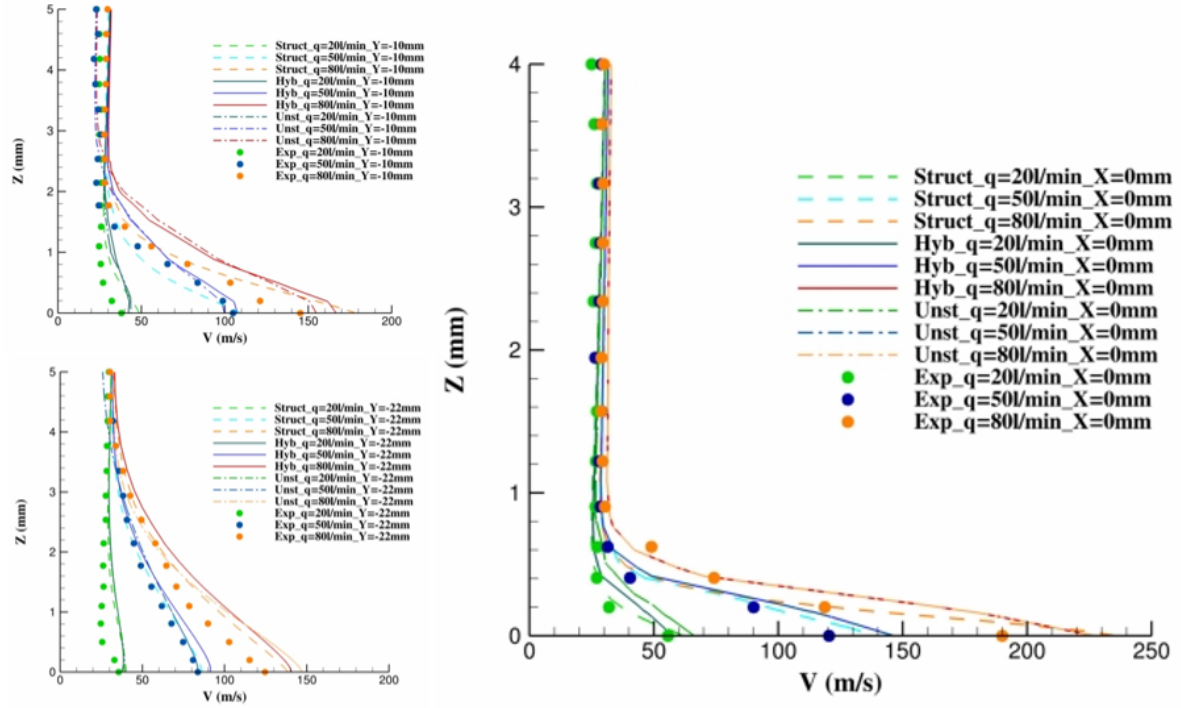

Figure 19: Velocity evolution for the different mesh approaches compared to experimental data

Table 2: Mesh numerical performance

	Structured	**Hybrid**	**Unstruct.**
Number of reference mesh cells (10^6)	16.0	33.29	33.29
Relative CPU cost (–)	1.0	1.0	1.61
Relative memory cost (–)	1.0	2.03	3.13

reference mesh providing excellent results in agreement with experimental data. Indeed, the structured multi-block strategy for the flat plate configuration offers better advantages than the other two strategies (unstructured and hybrid meshes) by considering convergence and numerical settings. The hybrid mesh was more difficult to generate unlike the structured mesh as a particular technique is necessary to execute the prism interface. Nevertheless, this method generates satisfying results compared to experimental data with a good compromise in terms of computational cost. In addition, it can be performed for complex geometries by meshing with unstructured approach and by preserving the quality of the structured mesh for simple geometries. The unstructured full is more expensive in terms of digital costs to implement. This option is therefore excluded to continue with a 360° configuration. According to these analysis, the simulations of the CME2 with injector will be based on hybrid mesh. These full annulus calculations using URANS combined with experimental measurements on the CME2 should provide further performance comparisons and flow topology assessments on the benefit of flow control.

5. Acknowledgments

The authors wish to thank the Consortium Research Industry in Turbomachinery members who support the study and also the members of ACONIT project for providing numerical database. The authors would like to thanks the french Defence Innovation Agency (AID) for co-funding this PhD. All simulations have been performed in the framework of the elsA agreement between SAFRAN and ONERA, which are co-owners of this software.

References

[1] Air Transport Action Group (ATAG). Waypoint 2050. 2021. https://www.atag.org/.

[2] J. Bae. *Active Control of Tip Clearance Flow in Axial Compressors. PhD thesis*. PhD Thesis, Massachusetts Institute of Technology, 2001.

[3] L. Cambier, S. Heib, and S. Plot. The Onera *elsA* CFD software: input from research and feedback from industry. *Mechanics & Industry*, 14:159–174, 1 2013.

[4] N. A. Cumpsty. Compressor aerodynamics. *Longman Scientific & Technical*, 1989.

[5] A. Deppe, H. Saathoff, and U. Stark. Spike-type stall inception in axial-flow compressors. *In 6th European Conference on Turbomachinery - Fluid Dynamics and Thermodynamics*, 2005.

[6] S. Geng, Z. Hongwu, J. Chen, and W. Huang. Tip clearance flow pattern in an isolated axial compressor rotor with micro tip injection. *In Proceedings of the 8th International Symposium on Experimental and Computational Aerothermodynamics of Internal Flows*, 2007.

[7] M. Kefalakis and K. D. Papailiou. Active flow control for increasing the surge margin of an axial flow compressor. *Proceedings of the ASME Turbo Expo*, 6 PART A:101–111, 2006. doi: 10.1115/ GT2006-90113.

[8] B.E. Launder and D.B. Spalding. The numerical computation of turbulent flows. *Computer Methods, Applied Mechanics and Engineering*, 3:269–289, 1974.

[9] J. Li, J. Du, S. Geng, F. Li, and H. Zhang. Tip air injection to extend stall margin of multi-stage axial flow compressor with inlet radial distortion. *Aerospace Science and Technology, Elsevier Masson SAS*, 96:105554, 2020.

[10] G. Margalida, P. Joseph, O. Roussette, et al. Active flow control in an axial compressor for stability improvement: on the effect of flow control on stall inception. *Experiments in Fluids*, 62(12), 2021. https://doi.org/10.1007/s00348-020-03104-4.

[11] J. Marty, L. Castillon, J-C. Boniface, S. Burguburu, and A. Godard. Numerical and experimental investigations of flow control in axial compressors. *AerospaceLab Journal*, 6:1-13, 2013. doi: 10.12762/2013.AL06-09.

[12] F. R. Menter. Two-equation eddy-viscosity turbulence models for engineering applications. *AIAA Journal*, 32(8):1598–1605, 1994.

[13] L. Neuhaus and W. Neise. Active control to improve the aerodynamic performance and reduce the tip clearance noise of axial turbomachines. *In AIAA Aeroacoustics Conference*, 2005.

[14] B. Smith. A near wall model for the k-l two equation turbulence model. *Fluid Dynamics Conference*, page 2386, 1994.

[15] P.R. Spalart and S.R. Allmaras. A one-equation turbulence model for aerodynamic flow. *In 30th Aerospace Science Meeting & Exhibit.*, pages 92–0439, 1992. AIAA.

[16] K. L. Suder, M. D. Hathaway, S. A. Thorp, A. J. Strazisar, and M. B. Bright. Compressor stability enhancement using discrete tip injection. *J. Turbomach*, 123:14, 2001.

[17] M. Veglio. *Etude expérimentale et numérique des écoulements dans un étage de compresseur axial à basse vitesse en régime de fonctionnement instable.* PhD Thesis, Ecole nationale supérieure d'arts et métiers - ENSAM, HAL Id: fftel-01345795, 2016. https://pastel.archives-ouvertes.fr/tel-01345795.